CONF-800744--5

ION-IMPLANTATION-INDUCED PHASE SEPARATION AND CRYSTALLIZATION IN LITHIA-SILICA GLASSES*

G. W. Arnold, P. S. Peercy, and B. L. Doyle
Sandia National Laboratories†
Albuquerque, New Mexico 87185

Abstract

Crystallization of annealed $Li_2O \cdot 2SiO_2$ glasses implanted with inert ions and fused SiO_2 glass implanted with Li ions was monitored using infrared reflection spectroscopy. Elastic recoil detection analysis was used to study changes in the Li and H concentration induced in these glasses by implantation and annealing. Implantation of $Li_2O \cdot 2SiO_2$ with inert ions results in Li depletion, accompanied by H indiffusion, in the implanted region. For Li-implanted SiO_2, crystallization of α-quartz is accompanied by appreciable Li diffusion to the surface and attendant H migration to the Li-depleted region. The crystallization mechanisms are discussed in terms of phase separation in the lithia-silica system.

*This work supported by the U. S. Department of Energy under Contract DE-AC04-76-DP00789.

†A U. S. Department of Energy facility.

DISCLAIMER

I. INTRODUCTION

It is well known that heating fused silica in the 1200 to 1700°C range results in coarse-grained cristobalite growth which nucleates at irregularities or surface impurities. We have previously shown[1] that crystallization of α-quartz in the near-surface region of high-purity fused silica can be produced by Li implantation followed by heat treatment at 700 to 800°C with a crystallite size typically on the order of one to five microns.

We have extended our investigation of ion-implantation-induced crystallization to lithium disilicate glass. The crystallization of lithia silicate glasses involves phase separation which occurs within a well-defined composition-temperature region.[2] Interstitial alkali ions can be removed from the near-surface region by the implantation of inert gas ions.[3-5] The composition and thus the phase separation characteristics of the near-surface region of the glass can be altered in a controlled manner by proper choice of the implanted ion, ion energy, and fluence.

In the present paper we report results of crystallization studies in $Li_2O \cdot 2SiO_2$ glass implanted with Xe and He and in Li-implanted fused silica glasses. The depth distributions of the implanted Li were measured using elastic recoil detection (ERD) analysis.[6] Structural changes in the implanted region ($\leq$ 1 μm in depth) were analyzed using infrared reflection spectroscopy (IRS). The ERD measurements also allow observation of the diffusion of hydrogen into the implanted region. Hydrogen distribution measurements are of interest because of changes in the corrosion resistance when hydrogen is incorporated into glass networks.[7,8]

As discussed below, the results for fused silica and lithium disilicate glass lead us to speculate that these two glasses can be viewed as end members of the lithia-silica glass system. From this viewpoint, implantation of

Li into pure SiO_2 produces separation of a Li-rich phase on a microscale in the glass upon which displaced SiO_2 network ions can precipitate. On the other hand, implantation of inert gas ions into $Li_2O \cdot 2SiO_2$ causes sufficient loss of Li from the near-surface region to permit phase separation and subsequent crystallization.

II. EXPERIMENTAL DETAILS

The $Li_2O \cdot 2SiO_2$ glass was cast from a melt (Pt crucible) of SiO_2 and Li_2CO_3 powders held at 1350°C for 24 hours and annealed at 300°C for one hour. Fused silica samples were prepared from Corning fused silica (CFS 7940). Implantation fluences from 5×10^{15} to 1×10^{17} ions/cm^2 were used at implantation energies of 250 keV (Xe), 100 keV (He) and 50 to 200 keV (Li). Thermal annealing was done in a tube furnace under flowing N_2, and the IRS measurements were made using a Beckman IR-12 spectrophotometer with a reflection attachment from N. J. Herrick, Inc.

The ERD analysis was performed using a 24 MeV ^{28}Si beam from Sandia's tandem Van de Graaff accelerator. The beam was incident at 75° to the sample normal and light ions recoiled at an angle 30° from the incident beam direction were detected. A 10 μm Al foil in front of the detector acted as a particle filter for the 24 MeV Si beams and also slowed the recoiled ions. Measurement of the recoil yield versus energy readily gives the light ion concentration versus depth. Detailed descriptions of the experimental arrangement and analysis have been given elsewhere.[6,9]

III. EXPERIMENTAL RESULTS

A. $Li_2O \cdot 2SiO_2$ Glasses

The infrared reflection spectrum of SiO_2 and of $Li_2O \cdot 2SiO_2$ is compared in Fig. 1. The major features in the SiO_2 spectrum are the Si-O-Si stretch

mode at 1115 cm^{-1} and the bending vibration at 800 cm^{-1}. Addition of Li_2O to form $Li_2O \cdot 2SiO_2$ produces bands near 1070 and 940 cm^{-1} which are characteristic of a homogeneous glass consisting of SiO_4 tetrahedra and Li_2O in which the presence of the Li_2O modifies the Si-O-Si stretching vibration and results in an Si-O dangling bond vibration near 940 cm^{-1}.

The IRS spectrum for $Li_2O \cdot 2SiO_2$ glass after implantation of 5×10^{15} and 1.1×10^{17} 250 keV Xe/cm^2 is shown in Fig. 2. The intensity of the Si-O-Si stretching vibration decreases as disorder is introduced and the Si-O-Si vibration shifts to higher energy while the Si-O vibration moves to lower energy. These energy shifts are associated with Li depletion as will be discussed below. Ferraro et al.[10] have seen similar shifts for glasses with Li_2O concentrations between $\sim$ 40 and 20 mole %. Spectral changes similar to those shown for Xe implantation in Fig. 2 are also observed for He implantation; however, the energy shifts are smaller indicating less Li depletion with He than with Xe.

A $Li_2O \cdot 2SiO_2$ glass sample implanted with 2×10^{16} 250 keV Xe/cm^2 was annealed at 500°C for various times. Indications of the tendency for phase separation are the appearance of the 1030 cm^{-1} absorption and the replacement of the 1070 cm^{-1} absorption with a relatively well-defined band at 1100 cm^{-1} after anneals of only 15 min.

Figure 3 shows that after an anneal of 20.5 hr. at 500°C, the spectrum contains sharp lines of crystalline $Li_2O \cdot 2SiO_2$ which have a one-to-one correspondence with the lines in the reference[11] spectrum of crystalline $Li_2O \cdot 2SiO_2$. Comparison of the data for the implanted side shows that the energy of the Si-O-Si stretching vibration increases continuously and the intensity of the 1030 cm^{-1} band grows monotonically with anneal time until the implanted region crystallizes. For this relatively long annealing time

the 1030 cm^{-1} band is observable on the unimplanted side. The $Li_2O \cdot 2SiO_2$ composition is very near the immiscibility boundary, and we attribute this incipient phase separation to result from the Li depletion commonly observed in the near-surface region of these glasses (see Fig. 4). Results qualitatively similar to those for Xe implantation have been obtained with He implantation.

The data of Figs. 1-3 and observations[12] of a Li-colloid band imply movement of Li ions in the near-surface region of implanted and annealed glasses, and we have used elastic recoil detection measurements to quantitatively evaluate these changes. ERD spectra for $Li_2O \cdot 2SiO_2$ are presented in Figs. 4-6. The ERD spectra contain the depth distribution information for both Li and H in the near-surface region. In the raw data, the signal from H in the glass is superimposed on the Li signal from the bulk; however, this background ERD yield has been subtracted from the H yield and the data have been corrected for the energy dependence of the scattering cross section to permit quantitative presentations of concentration versus depth. The spectra in Fig. 4 give the Li depth distribution before implantation and after implantation of 5×10^{16} 250 keV Xe/cm^2 and after a 500°C anneal. Note that the Li distribution is not uniform very near the surface in the unimplanted glass. There is evidence for Li depletion in the first $\sim$ 3000 Å; in this region the Li has apparently been replaced by H (see Fig. 6). After implantation with Xe there is a pronounced dip in the Li concentration at a depth of $\sim$ 1500 Å below the surface, which is near the Xe projected range. The He-implanted samples also show an increase in the Li concentration at the surface. After the 500°C anneal the enhanced Li concentration near the surface has disappeared; furthermore, there is a uniform reduction of Li in the bulk of $\sim$ 15% throughout the $\sim$ 6000 Å depth probed.

The H depth distribution in these same Xe-implanted samples is shown in Fig. 5. Before implantation, the H distribution extends $\sim$ 3000 Å into the sample with a peak concentration in the first $\sim$ 2000 Å of $\sim$ 17 at.%. This H depth profile depends on the sample history and presumably results from H indiffusion as is well-known from studies of weathering in glasses.[7,8] These particular samples were polished $\sim$ 18 months before the ion implantation and ERD measurements were performed. After 5×10^{16} 250 keV Xe/cm^2 implantation, the H redistributes in the implanted region. This H motion is presumably due to Li motion and the H partially compensates the Li loss. While the H compensation appears to be essentially complete for the "weathered" surface before implantation, the compensation during implantation is limited by a fixed supply of H, i.e., the H which was initially in the sample.

We have found[12] analogous results for He implantation in which most of the energy is deposited into electronic processes. As in the case with Xe implantation, He implantation produces an appreciable migration of Li toward the surface. In fact, the Li concentration approaches the stoichiometric value at the surface after implantation of 1×10^{17} He/cm^2 in contrast to the Li depletion observed before the implant. A loss of Li from both the near-surface and bulk, completely analogous to the results for Xe implantation, is observed after annealing at 500°C. A further striking example of the depletion of near-surface alkali ions and their replacement by surface H, after inert-gas ion bombardment, is shown in Fig. 7. A sample of glass with composition 88% SiO_2 and 12% K_2O was prepared and implanted with 7×10^{16} 250 keV Xe^+ ion/cm^2. Before implantation the spectral features are the main Si-O-Si stretch near 1100 cm^{-1} and a weak band at $\sim$ 940 cm^{-1}. The latter is associated with non-bridging oxygen ions in an alkali-rich environment.[13] After implantation the $\sim$ 940 cm^{-1} band is replaced by a band at $\sim$ 980 cm^{-1}. This

is the Si-OH dangling bond[13] and shows that as alkali is depleted by the bombardment, H from the surface replaces it to form the Si-OH species.

The combined results for the Li and H distributions in the $Li_2O \cdot 2SiO_2$ glasses and the results of Fig. 7 conclusively demonstrate that Li outdiffusion is accompanied by H indiffusion after inert ion implantation. These observations support the suggestion that alkali diffusion is governed by chemical[14] and electrostatic forces.[15]

B. Fused Silica

Measurements of Li motion associated with the crystallization of α-quartz induced by Li implantation and annealing were made for comparison with the observations in the $Li_2O \cdot 2SiO_2$ system. The 24 MeV ^{28}Si ERD spectra for CFS 7940 SiO_2 implanted with 1×10^{17} 50 keV Li/cm^2 for an as-implanted sample and after a 15 min. anneal at 600°C are shown in Fig. 8. The as-implanted Li distribution consists of two peaks, with the more shallow peak occurring near the predicted LSS range of 2000 Å and a broader distribution peaked near 4500 Å. There is no observable change in the Li depth distribution after a 600°C anneal. Similar double-peaked profiles were previously observed[3,4] for Ag implantation into LAS glasses. Such distributions are attributed to the motion of high mobility ions induced by sample heating by the implant beam. It was found in the studies of Ag that this distribution could be altered by changing the beam current or by reducing the sample temperature. For Ag implants with the sample temperature at 77°K, the distribution approached a Gaussian distribution centered about the expected Ag ion range.

Although no change in the Li distribution is observed for 600°C anneals, which is below the temperature required for the onset of α-quartz crystallization, changes in the Li profile are observed for higher annealing temperatures. The effects of annealing at 700 and 800°C on the implanted Li profile

are shown in Fig. 9. After a 15 min. anneal at 700°C the Li distribution has changed markedly. The Li peak at ∿ 2000 Å has essentially disappeared and the Li concentration in the 4500 Å peak is reduced while a significant accumulation of Li at the surface is observed. Annealing at 800°C further increases the Li concentration near the surface. Indeed, after an 800°C anneal, 30% of the Li migrated from the bulk to the surface; however, the bulk concentration of Li is still appreciable, and it is presumably this Li which forms Li_2O nuclei that permit the growth of crystalline α-quartz.

As Li migrates in SiO_2 during annealing, there is attendant H motion analogous to that observed for the $Li_2O \cdot 2SiO_2$. The H depth distribution in Li-implanted SiO_2 is shown before annealing and after the 700°C anneal in Fig. 10. Before annealing there is H very near the surface, and the H content of the bulk is much less for SiO_2 than that shown previously for the $Li_2O \cdot 2SiO_2$ glass. The bulk H concentration is 1.4×10^{20} H/cm^3, which is in good agreement with the value of 1.3×10^{20} H/cm^3 found by Allred et al.[15] for Suprasil fused SiO_2 glass. Surface hydrogen is always observed and it is probable that the H observed in the as-implanted sample was introduced during polishing and/or implantation. After the 700°C anneal, however, H migrates in the bulk of SiO_2 and peaks occur in the H distribution near the same depths that the peaks in the Li distribution were observed. Thus, as in the case for $Li_2O \cdot SiO_2$ glass, Li migration to the surface is accompanied by H indiffusion. It should also be noted that the total H content in the implanted region is greater after the 700°C anneal than for the as-implanted case, but that the H content in the 1000 to 5000 Å depth region is less than the Li depletion from this region.

IV. DISCUSSION

A. Crystallization of $Li_2O \cdot 2SiO_2$ Glasses

The temperature-composition range in which phase separation occurs in the $Li_2O \cdot 2SiO_2$ system is shown in Fig. 11. Since the Li_2O content of $Li_2O \cdot 2SiO_2$ is above the Li_2O content of the immiscibility boundary, no phase separation is expected for $Li_2O \cdot 2SiO_2$. However, if the Li_2O content were decreased by $\leq$ 2 mole %, phase separation could be expected for temperature $\leq$ 500°C. The present experiments clearly demonstrate that inert ion implantation depletes the Li concentration in the implanted region. These data further show that the Li depletion in the implanted region is sufficient to yield a composition well within the immiscibility boundary for the temperatures under consideration. A question remains as to the local O content in the implanted glass. We have no evidence that O is lost during implantation; however, the ERD measurements show that the Li depletion is compensated by H which presumably saturates dangling O bonds and the data of Fig. 7 clearly show the attachment of H to non-bonding oxygen. The net effect of implantation of $Li_2O \cdot 2SiO_2$ glass with Xe and He is thus to reduce the Li_2O content so that the resulting composition is well within the immiscibility boundary. Upon annealing at 500°C, the implanted region crystallizes whereas the unimplanted region does not show evidence of crystallization.

It was noted in Section III A that, from the infrared reflection measurements there appeared to be tendency for phase separation in the unimplanted side of the $Li_2O \cdot 2SiO_2$ glasses after annealing at 500°C. This phase separation is also understandable within the framework of the above discussion of implantation-induced crystallization. As the data in Figs. 4 and 5 show, the Li has been depleted to a $\sim$ 3000 Å depth and replaced by H in the normal weathering process. Such Li depletion again moves the composition within the immiscibility boundary

where phase separation is expected. Indeed, it would not be surprising to find evidence for crystallization under annealing in this near-surface region, although no such evidence was found in the present measurements.

B. Crystallization of α-Quartz from SiO_2

The details of the Li-induced crystallization of SiO_2 glass to produce α-quartz are not as clear as those for the crystallization of $Li_2O \cdot SiO_2$. Implantation of Li into SiO_2 glass has at least two consequences: (1) Introduction of Li changes the chemical composition of the glass, and (2) The ion-implantation process introduces damage in the glass. In particular, near the end of range, the Li ions produce a region of intense displacement damage as much of their energy is expended in nuclear collision processes. The atomic displacement damage results in oxygen vacancies in fused SiO_2 as has been measured[16] by UV absorption near 2450 Å of O vacancies with trapped electrons after implantation of Li, B, or Al. The O vacancies recombine with interstitials as the radiation damage anneals at temperatures near 700 to 800°C, which is the same temperature region for which α-quartz is observed[1] to crystallize.

In addition to the effects of implantation-induced disorder, the implanted Li concentration appears to be important to the crystallization process. No evidence for crystallization has been observed for implantation of the network ions Si and O or for implantation with the network-forming ions Al and B. Similarly, we have been unable to induce crystallization by implantation of the alkali ion Na. It is not clear why no crystallization was observed with Na, which is chemically similar to Li, but the fact that the mobility[17] of Na is ∿ 25 times that of Li at 350°C may allow the Na to migrate too readily during implantation and annealing to form nuclei.

For an implant of $1x10^{17}$ 50 keV Li/cm^2, the Li concentration at depths from $\sim$ 1000 to 5000 Å was measured to be $\sim 0.3x10^{22}$ Li/cm^3. If all of this Li were to bond as Li_2O, the local Li_2O concentration could be as high as 7 mole %. For these compositions it is theoretically possible for there to be phase separation of small $Li_2O \cdot 2SiO_2$ particles within an SiO_2-rich host. If this were indeed the case, then the primary role of Li in the crystallization process is to form nuclei and to prevent the SiO_4 tetrahedra from recombining into the glass network before the crystallization temperature is reached. As the α-quartz crystallizes with the recombination of implantation-induced interstitial-vacancy complexes, much of the Li becomes superfluous and is swept to the surface. In this regard it is significant that no Li motion is observed for annealing temperatures below 700°C, where crystallization begins. At that temperature Li is lost primarily from the 2000 Å depth region, i.e., from end of range where the majority of the displacement damage was produced. If these suggestions are correct, then the implantation-induced crystallization of both $Li_2O \cdot 2SiO_2$ and SiO_2 glasses can be understood on the basis of phase separation in the lithia-silicate system.

V. CONCLUSIONS

We have shown that ion implantation can be used to selectively crystallize the near-surface regions of glasses and have discussed the crystallization in terms of the lithia-silica phase diagram. Ion implantation is used to alter the composition of the near-surface region, and crystallization is preferentially limited to the implanted areas of the glass. For the lithium disilicate glass system, implantation of inert ions depletes the near-surface region of Li until the composition within the implanted region falls within the immiscibility boundary. Crystallization then occurs when the glass is heated to

500°C. For pure fused SiO_2 glass, implantation of Li followed by heat treatment at 700 to 800°C results in the crystallization of α-quartz. Crystallization of this system was also discussed in terms of the lithia-silica phase diagram and it was suggested that crystallization in this system might also be governed by this diagram.

The motion of Li and H during the annealing process was measured by ERD spectroscopy. These measurements afford the first quantitative evaluation of the interrelation between Li and H during crystallization in these systems and show that Li depletion in both $Li_2O \cdot 2SiO_2$ and Li implanted SiO_2 is accompanied by H indiffusion. These measurements further show that crystallization of α-quartz from fused SiO_2 takes place with simultaneous motion of Li from the end-of-range depth to the surface. These results provide new insight into the crystallization processes and associated ion motion and may have important applications in the study of weathering and corrosion.

REFERENCES

1. G. W. Arnold, in: Proceedings of International Conference on Ion Beam Modification of Materials, 4-8 September, 1978, Budapest, Hungary, ed. J. Gyulai, T. Lohner, and E. Pasztor (1979) 929; Rad. Eff. 47, (1980) 15.
2. See, e.g., H. J. Stevens, in: Introduction to Glass Science, ed. L. D. Pye, H. J. Stevens, and W. C. LaCourse, Plenum Press (1972) 237; M. Tomazawa, in: Treatise on Materials Science and Technology 17, Glass II, ed. M. Tomazawa and R. H. Doremus, Academic Press (1979) 71.
3. G. W. Arnold and J. A. Borders, J. Appl. Phys. 48 (1977) 1488.
4. G. W. Arnold and J. A. Borders, in: Applications of Ion Beams to Material, 1975, ed. G. Carter, J. S. Collingon, and W. A. Grant, Conference Series No. 28, The Institute of Physics, London (1976) 121.
5. J. A. Borders and G. W. Arnold in: Proceedings of International Conference on Ion-Beam Surface Layer Analysis, Karlsruhe, Germany, 1975, ed. O. Meyer, G. Linker, and S. Käppaler, Plenum Press (1976) 415.
6. B. L. Doyle and P. S. Peercy, Appl. Phys. Lett. 34, 811.
7. W. A. Lanford, K. Davis, P. Lamarche, T. Laursen, R. Groleau, and R. H. Doremus, J. Non-Cryst. Sol. 33 (1979) 249.
8. R. H. Doremus, J. Non-Cryst. Sol. 19 (1975) 137.
9. B. L. Doyle and P. S. Peercy, Proceedings of BES/DOE Workshop, The Analysis of Hydrogen in Solids, ed. by R. L. Schwoebel and J. L. Warren, DOE/ER-0026 (U. S. Department of Energy, Washington, DC, 1979) 92.
10. J. R. Ferraro, M. H. Maghnani, and L. J. Basile, J. Appl. Phys. 44 (1973) 5391.
11. R. A. Nyquist and R. O. Kagel, Infrared Spectra of Inorganic Compounds (3800-45 cm^{-1}), Academic Press (1971) 91.

12. G. W. Arnold and P. S. Peercy, J. Non-Cryst. Sol. (to be published).

13. G. W. Arnold, Proceedings of International Conference on MOS Insulators, Raleigh, NC, 18-20 June, 1980 (to be published).

14. D. V. McCaughan and R. A. Kushner, in: Characterization of Solid Surfaces, ed. P. F. Kane and G. B. Larrabee, Plenum Press (1974) 627.

15. D. D. Allred, C. W. White, G. J. Clark, B. R. Appleton, and I. S. T. Tsong, in: The Physics of SiO_2 and its Interfaces, ed. S. T. Pantelides, Pergamon Press (1978) 210.

16. G. W. Arnold, IEEE Trans. Nucl. Sci. NS-20 (1973) 220.

17. R. H. Doremus, Phys. Chem. Glasses 10 (1969) 28.

FIGURE CAPTIONS

Fig. 1. Comparison of the IRS spectra of SiO_2 glass (CFS 7940) and lithium disilicate glass for the spectral region between 700 and 1300 cm^{-1}.

Fig. 2. Reflectance spectra for $Li_2O \cdot 2SiO_2$ glass after implantation with $5x10^{15}$ and $1.1x10^{17}$ 250 keV Xe/cm^2.

Fig. 3. Reflectance spectra for implanted ($2x10^{16}$ 250 keV Xe/cm^2) and unimplanted (reverse side of sample) $Li_2O \cdot 2SiO_2$ glass after a 20.5 hr. anneal at 500°C.

Fig. 4. Li depth distribution of $Li_2O \cdot 2SiO_2$ measured by ERD showing the effect of $5x10^{16}$ 250 keV Xe/cm^2 implantation and a subsequent thermal anneal at 500°C.

Fig. 5. H depth distribution measured by ERD for the sample of Fig. 4.

Fig. 6. Comparison of the Li and H profiles in the near-surface region of $Li_2O \cdot 2SiO_2$ implanted with $5x10^{16}$ 250 keV Xe/cm^2.

Fig. 7. Reflectance spectra for implanted ($7x10^{16}$ 250 keV Xe^+/cm^2) and unimplanted 88% SiO_2:12% K_2O glass.

Fig. 8. Li depth distribution in CFS 7940 SiO_2 after implantation of $1x10^{17}$ 50 keV Li/cm^2 at room temperature and after annealing at 600°C.

Fig. 9. Change in the Li profile in SiO_2 implanted with $1x10^{17}$ 50 keV Li/cm^2 after anneals at 700 and 800°C.

Fig. 10. H distribution in SiO_2 implanted with $1x10^{17}$ 50 keV Li/cm^2 and after annealing at 700°C.

Fig. 11. Phase diagram of the lithia-silica system showing the region of phase separation. After M. Tomazawa, Phys. Chem. Glasses 14 (1973) 112.

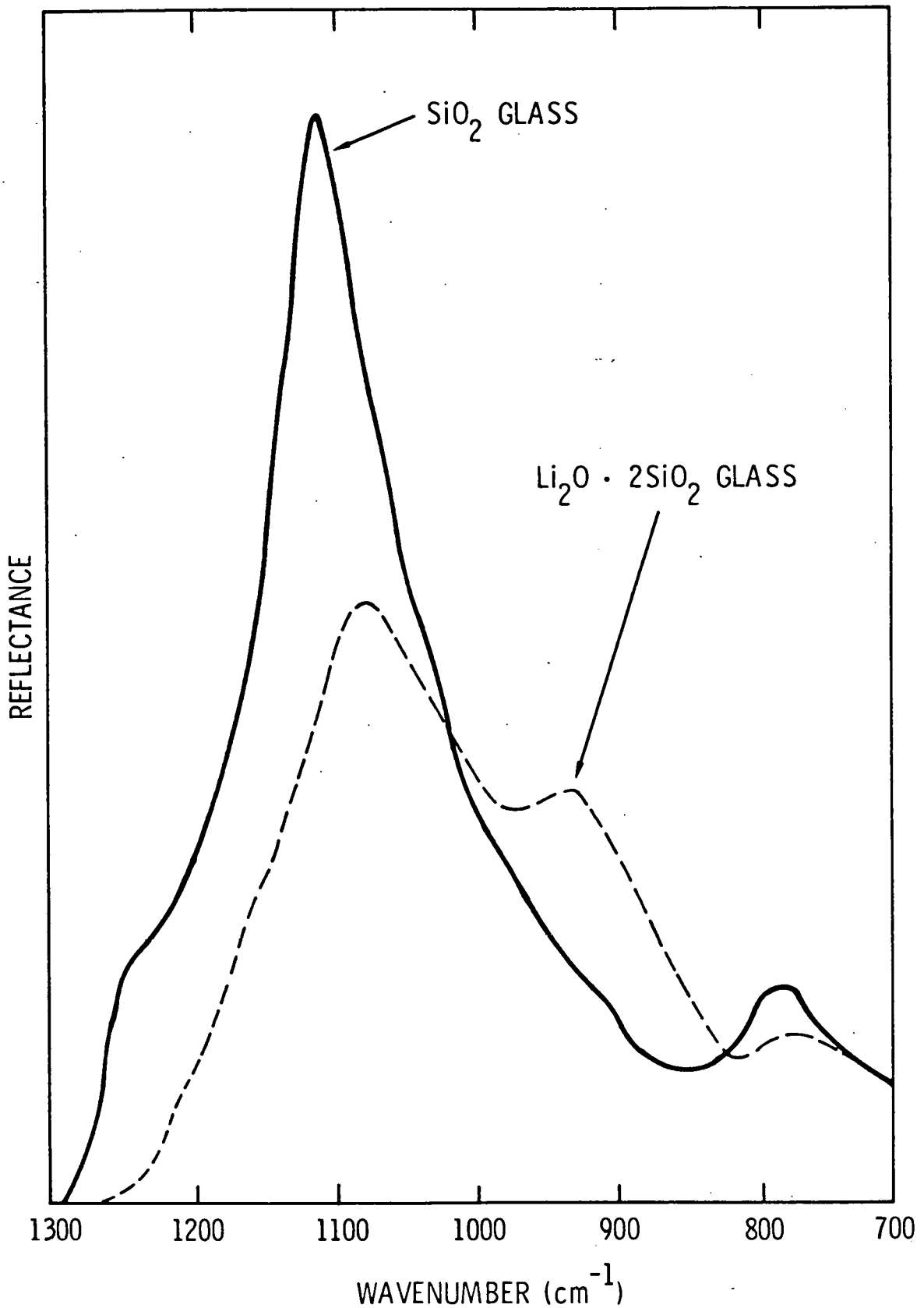
SiO_2 GLASS
$Li_2O \cdot 2SiO_2$ GLASS
REFLECTANCE
1300
1200
1100
1000
900
800
700
WAVENUMBER (cm^{-1})

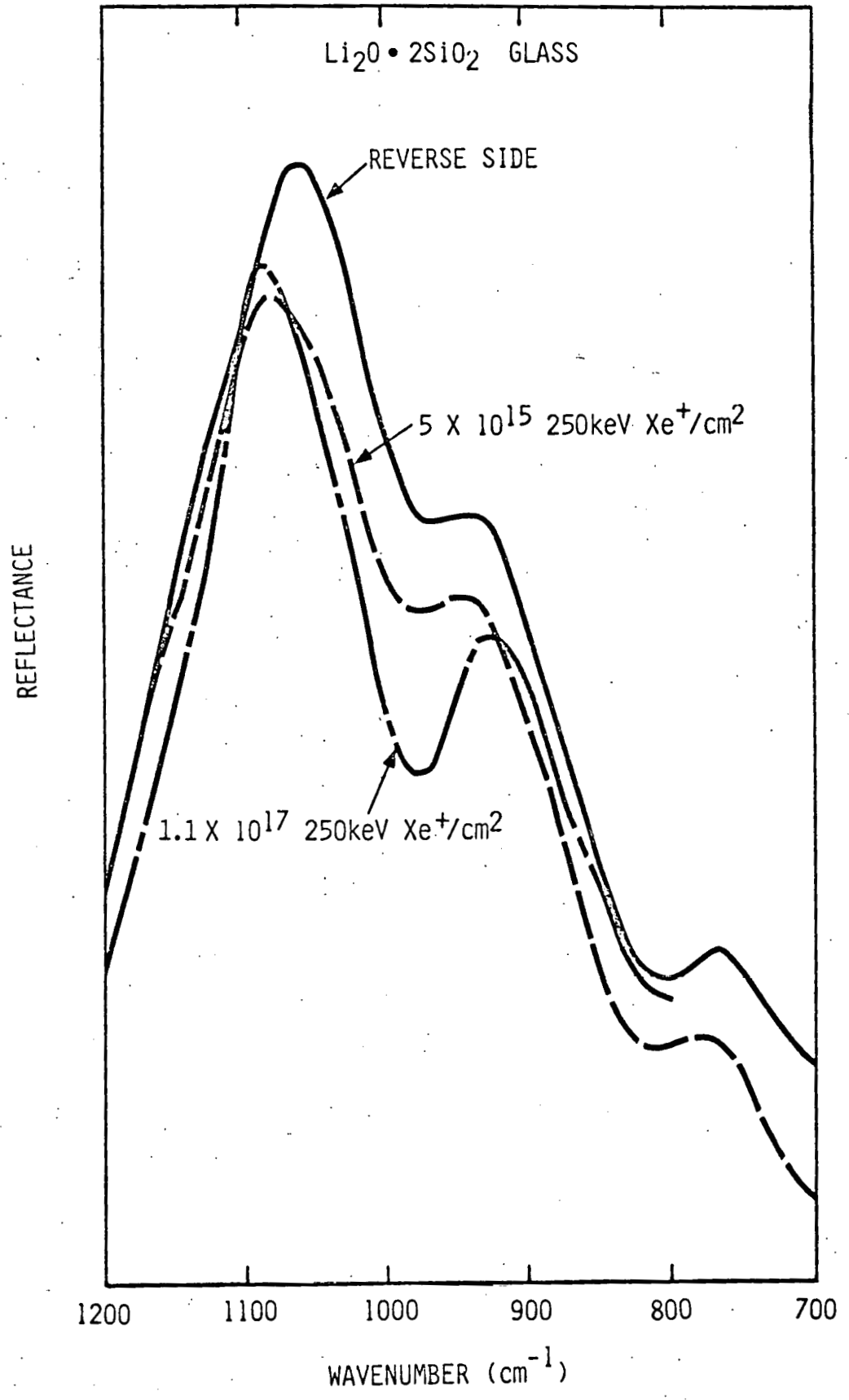
$Li_2O \cdot 2SiO_2$ GLASS
REVERSE SIDE
5 X 10^{15} 250keV Xe^+/cm^2
1.1 X 10^{17} 250keV Xe^+/cm^2
REFLECTANCE
1200
1100
1000
900
800
700
WAVENUMBER (cm^{-1})

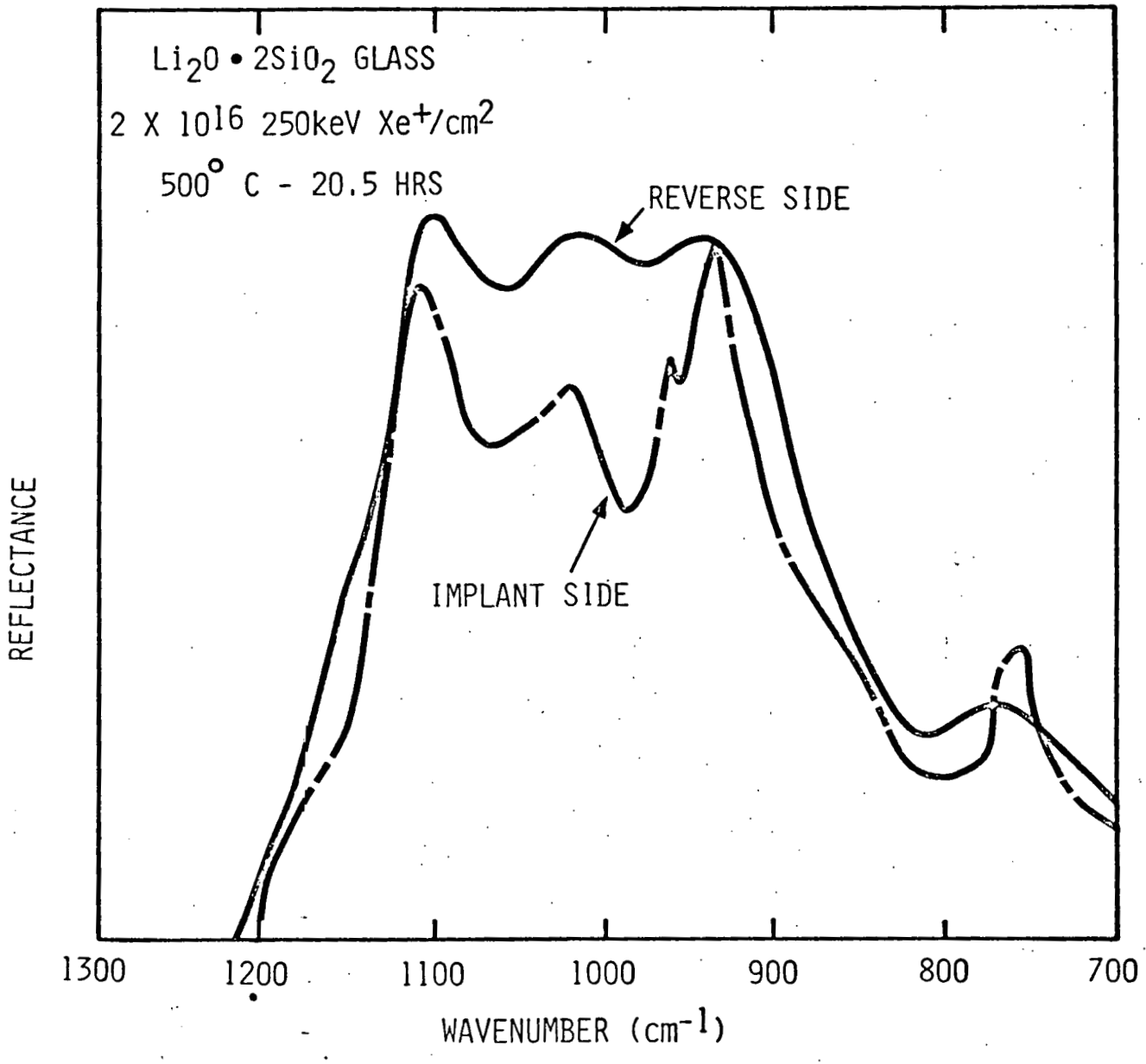
$Li_2O \cdot 2SiO_2$ GLASS
2 X 10^{16} 250keV Xe^+/cm^2
500° C - 20.5 HRS
REVERSE SIDE
IMPLANT SIDE
REFLECTANCE
1300
1200
1100
1000
900
800
700
WAVENUMBER (cm^{-1})

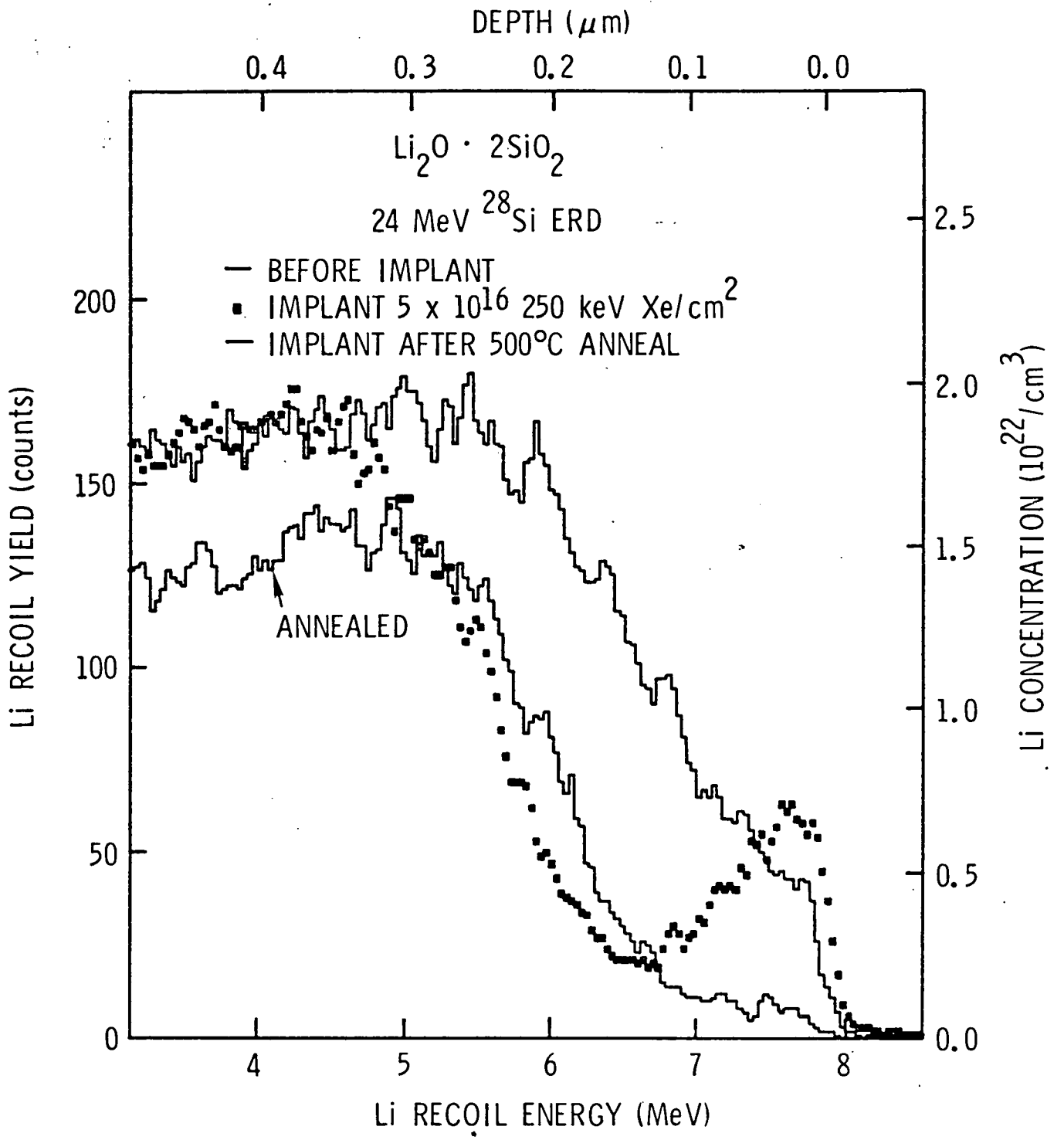
DEPTH (μm)
0.4
0.3
0.2
0.1
0.0
$Li_2O \cdot 2SiO_2$
24 MeV ^{28}Si ERD
— BEFORE IMPLANT
▪ IMPLANT 5 x 10^{16} 250 keV Xe/cm^2
— IMPLANT AFTER 500°C ANNEAL
ANNEALED
Li RECOIL YIELD (counts)
200
150
100
50
0
Li CONCENTRATION (10^{22}/cm^3)
2.5
2.0
1.5
1.0
0.5
0.0
4
5
6
7
8
Li RECOIL ENERGY (MeV)

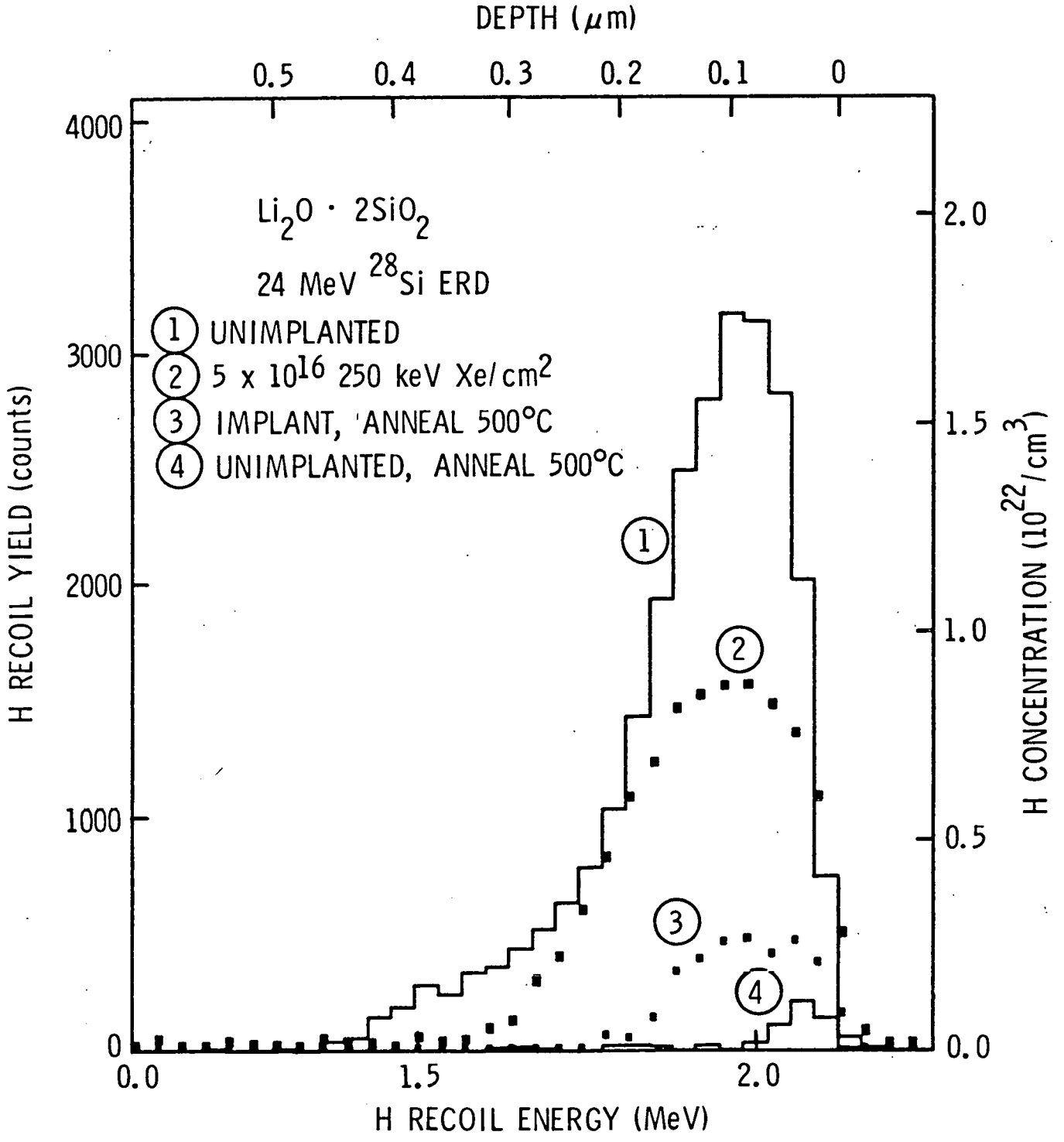
DEPTH (μm)
0.5
0.4
0.3
0.2
0.1
0
4000
3000
2000
1000
0
$Li_2O \cdot 2SiO_2$
24 MeV ^{28}Si ERD
1 UNIMPLANTED
2 5 x 10^{16} 250 keV Xe/cm^2
3 IMPLANT, ANNEAL 500°C
4 UNIMPLANTED, ANNEAL 500°C
H RECOIL YIELD (counts)
2.0
1.5
1.0
0.5
0.0
H CONCENTRATION (10^{22}/cm^3)
0.0
1.5
2.0
H RECOIL ENERGY (MeV)

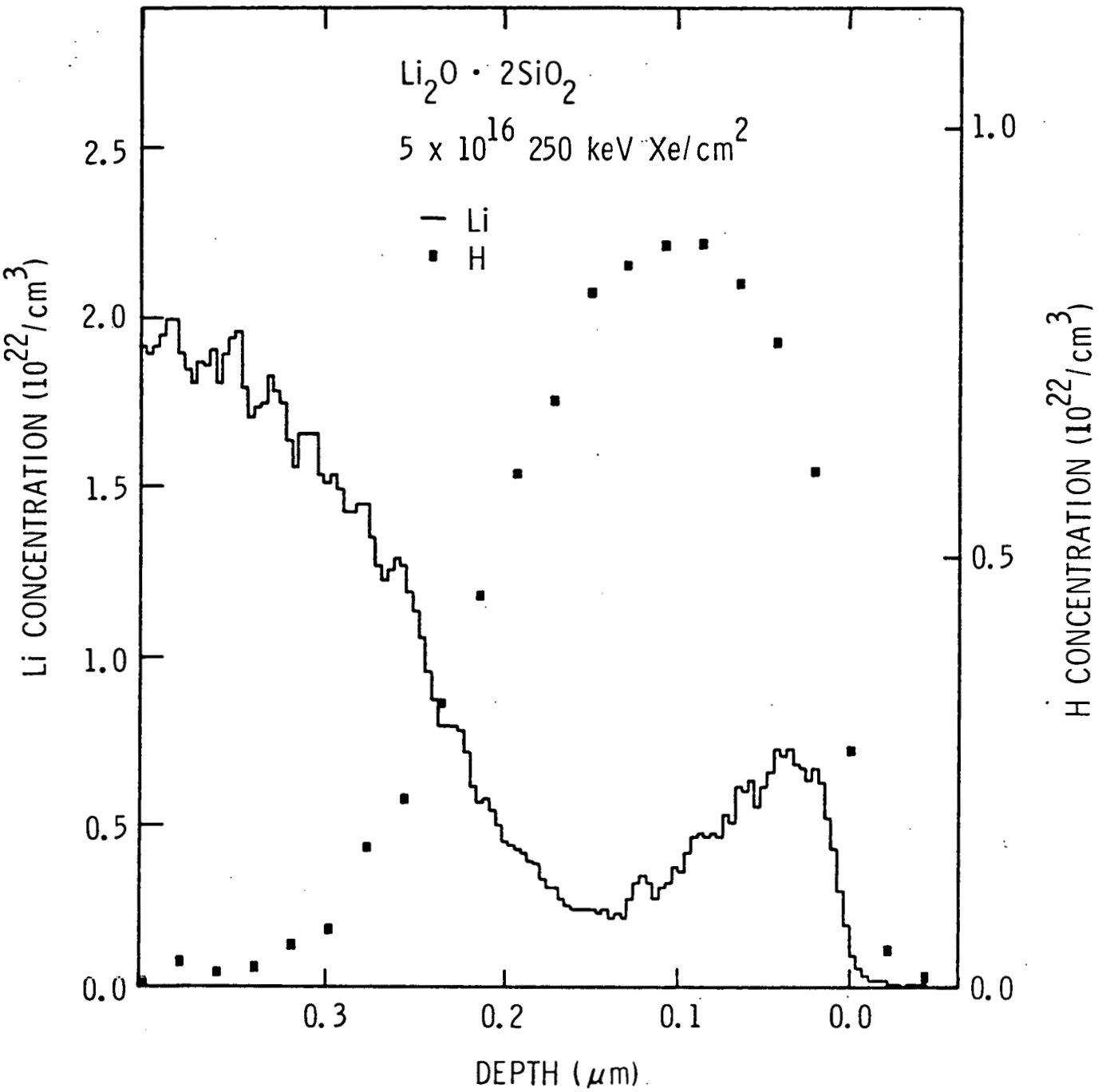
$Li_2O \cdot 2SiO_2$
5×10^{16} 250 keV Xe/cm^2
Li
H
Li CONCENTRATION (10^{22}/cm^3)
H CONCENTRATION (10^{22}/cm^3)
DEPTH (μm)
2.5
2.0
1.5
1.0
0.5
0.0
0.3
0.2
0.1
0.0

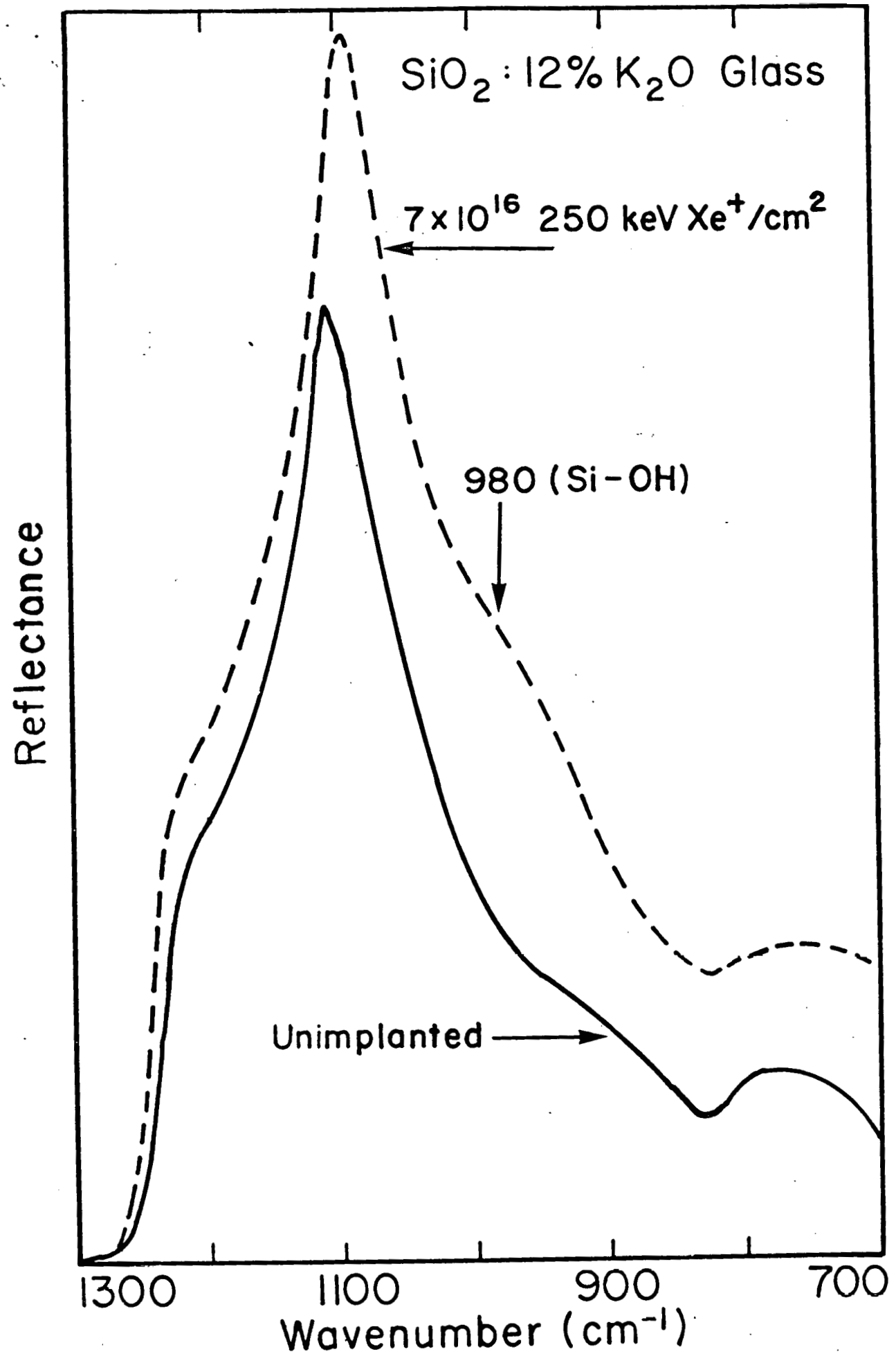
SiO_2 : 12% K_2O Glass
7×10^{16} 250 keV Xe^+/cm^2
980 (Si-OH)
Unimplanted
Reflectance
1300
1100
900
700
Wavenumber (cm^{-1})

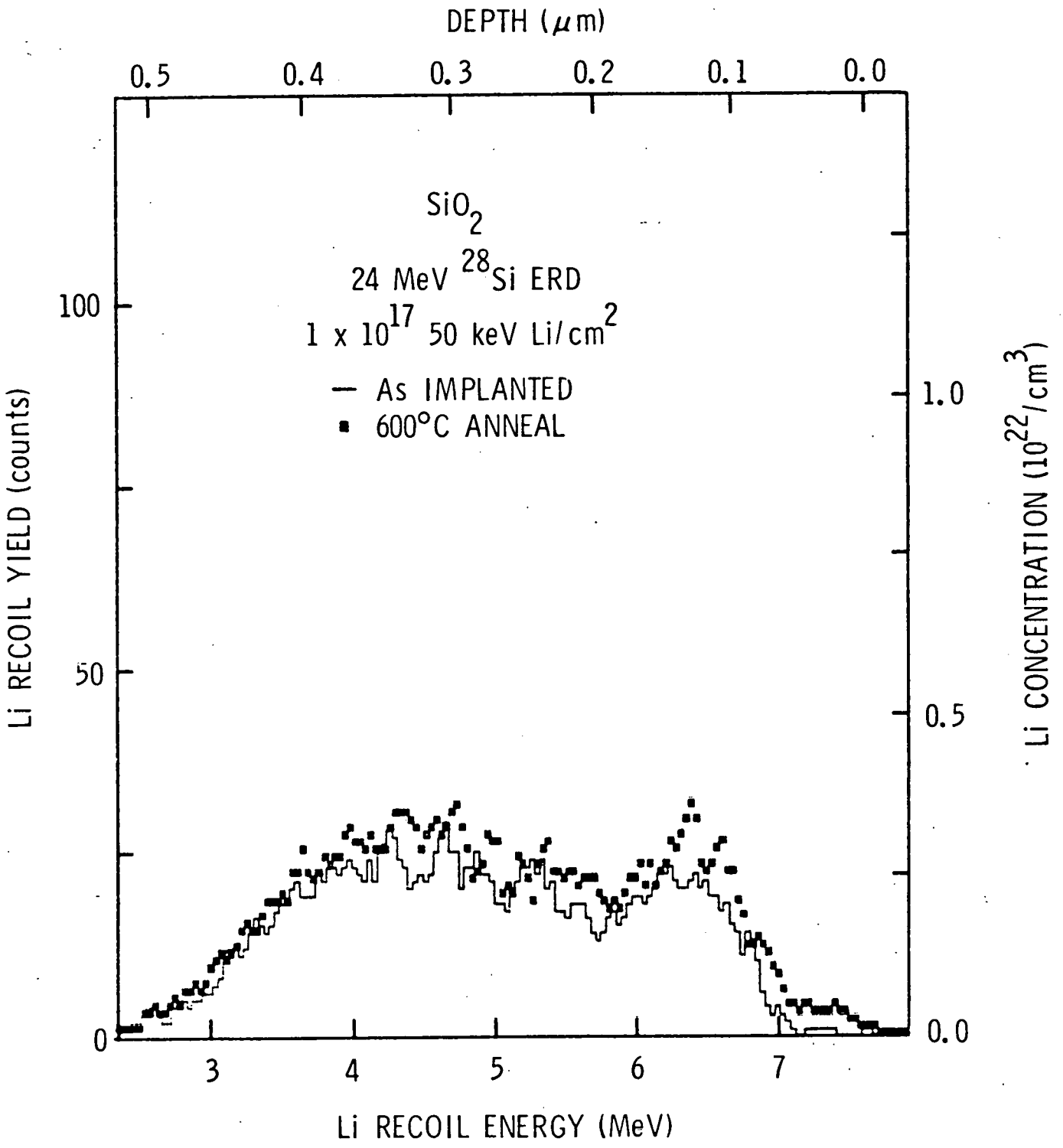
DEPTH (μm)
0.5
0.4
0.3
0.2
0.1
0.0
SiO2
24 MeV 28Si ERD
1 x 10^17 50 keV Li/cm^2
— As IMPLANTED
▪ 600°C ANNEAL
100
50
0
Li RECOIL YIELD (counts)
1.0
0.5
0.0
Li CONCENTRATION (10^22/cm^3)
3
4
5
6
7
Li RECOIL ENERGY (MeV)

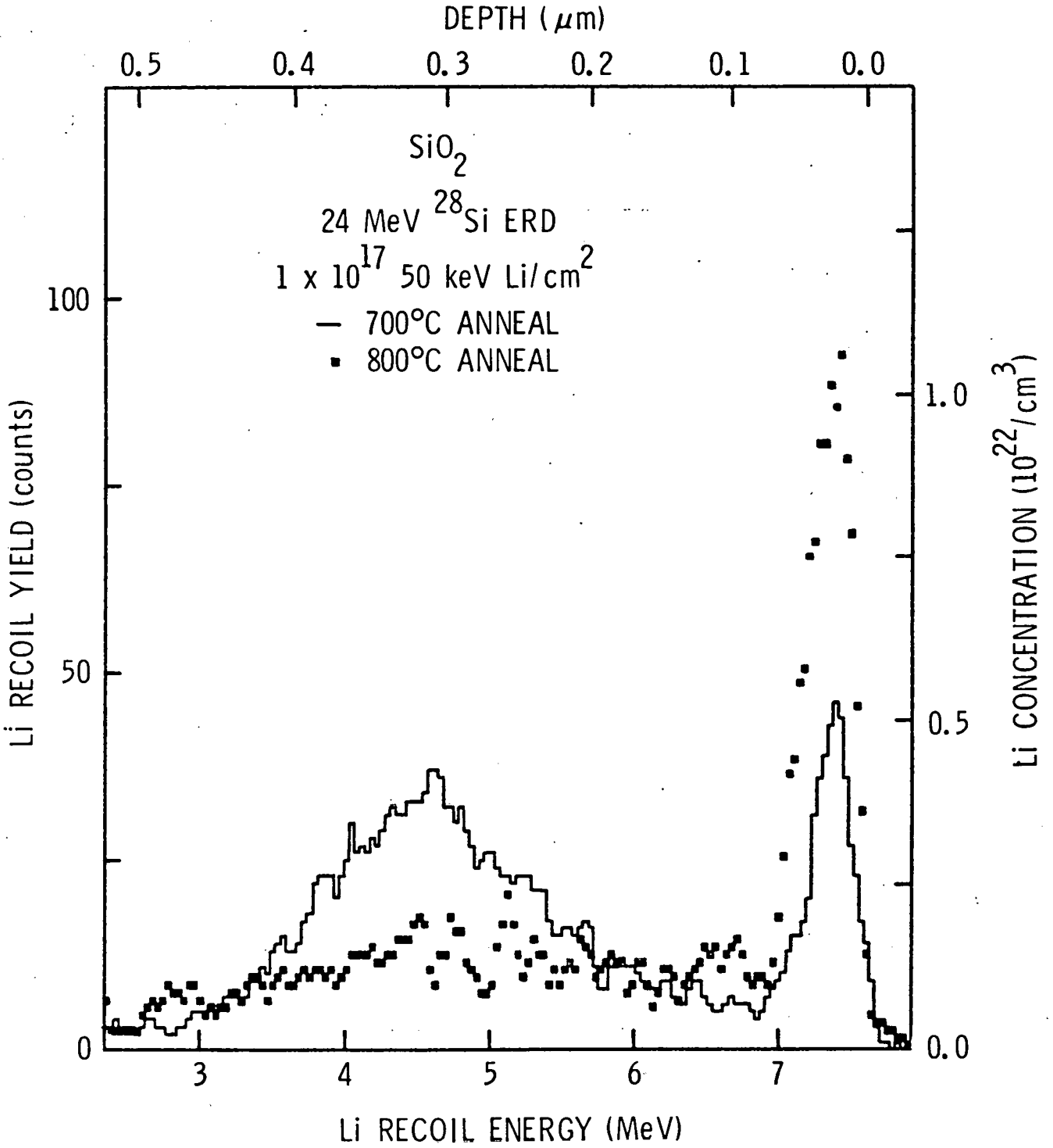
DEPTH (μm)
0.5
0.4
0.3
0.2
0.1
0.0
SiO2
24 MeV 28Si ERD
1 x 10^17 50 keV Li/cm^2
— 700°C ANNEAL
▪ 800°C ANNEAL
100
50
0
Li RECOIL YIELD (counts)
1.0
0.5
0.0
Li CONCENTRATION (10^22/cm^3)
3
4
5
6
7
Li RECOIL ENERGY (MeV)

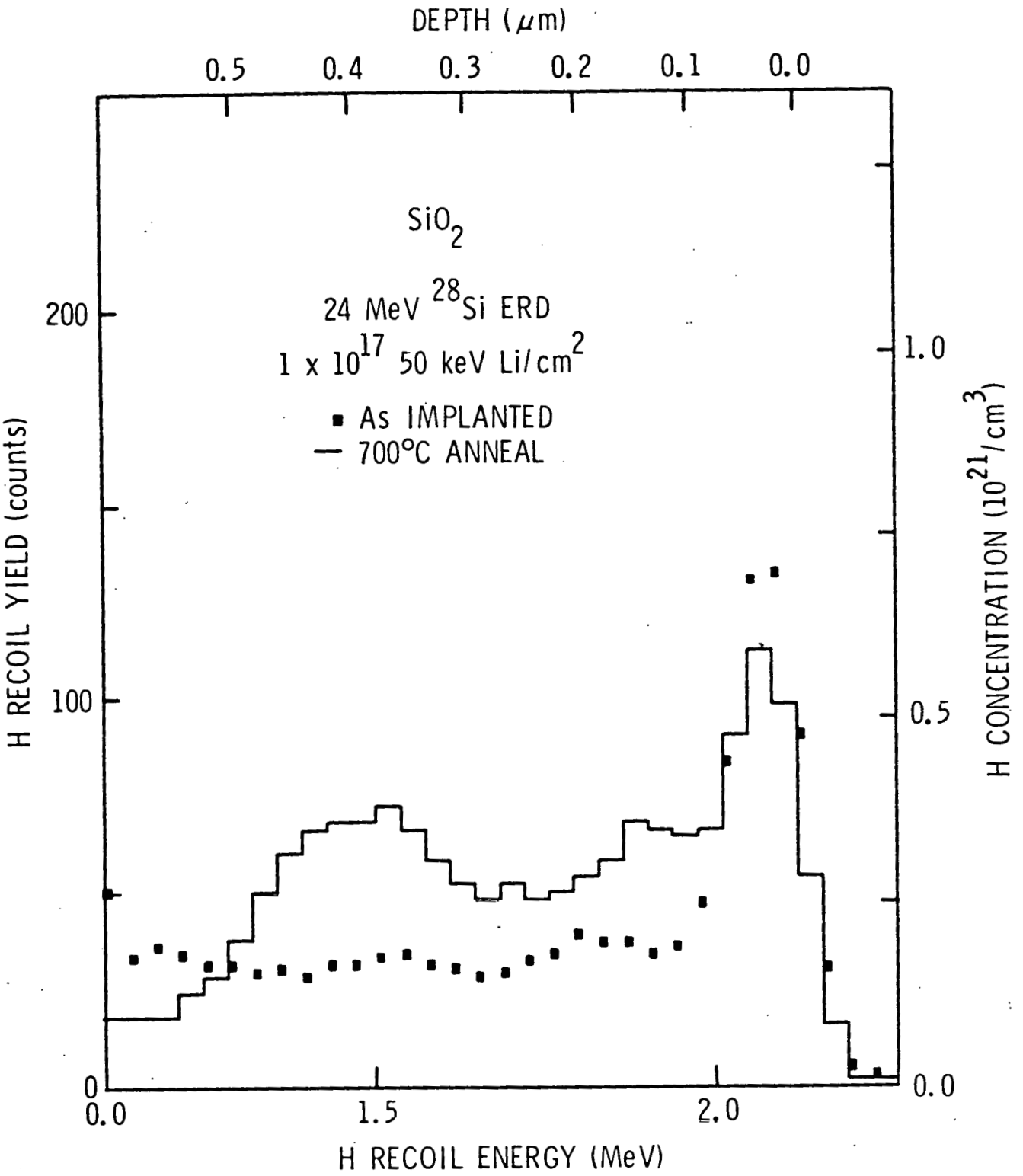
DEPTH (μm)
0.5
0.4
0.3
0.2
0.1
0.0
SiO2
24 MeV 28Si ERD
1 x 10^17 50 keV Li/cm^2
As IMPLANTED
700°C ANNEAL
H RECOIL YIELD (counts)
200
100
0
H CONCENTRATION (10^21/cm^3)
1.0
0.5
0.0
0.0
1.5
2.0
H RECOIL ENERGY (MeV)

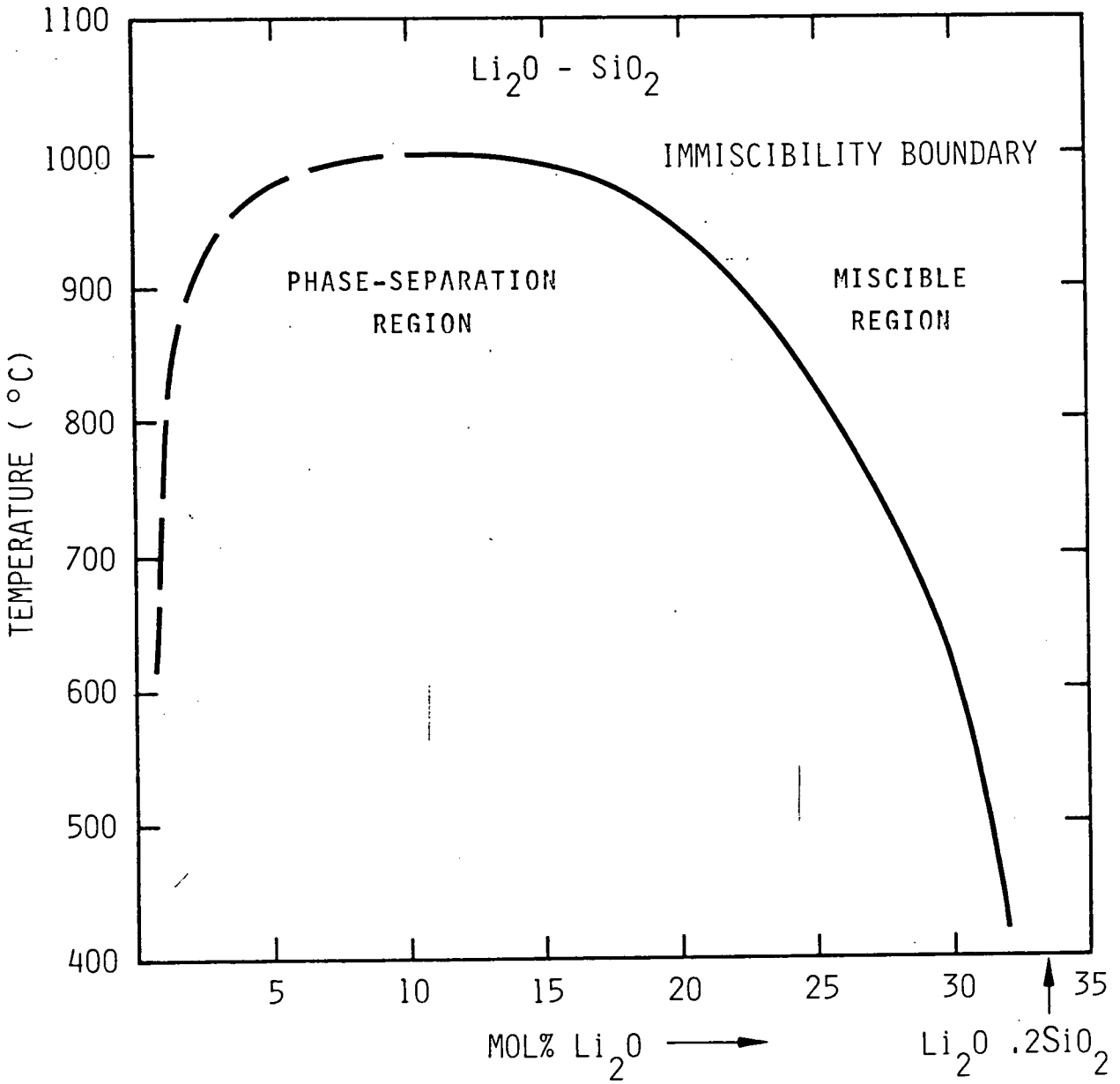
Li_2O - SiO_2
IMMISCIBILITY BOUNDARY
PHASE-SEPARATION REGION
MISCIBLE REGION
TEMPERATURE (°C)
1100
1000
900
800
700
600
500
400
5
10
15
20
25
30
35
MOL% Li_2O
Li_2O .$2SiO_2$